Available online at http://scik.org
Commun. Math. Biol. Neurosci. 2020, 2020:29
https://doi.org/10.28919/cmbn/4550
ISSN: 2052-2541

SIS MULTI-REGIONS DISCRETE INFLUENZA PANDEMIC MODEL AND TRAVEL-BLOCKING VICINITY OPTIMAL CONTROL STRATEGY ON TWO FORMS OF PATCH

BOUTAYEB HAMZA, BIDAH SARA, ZAKARY OMAR*, ELMOUKI ILIAS, FERJOUCHIA HANANE, RACHIK MOSTAFA

Laboratory of Analysis Modelling and Simulation, Department of Mathematics and Computer Science, Faculty of Sciences Ben M'Sik, Hassan II University of Casablanca, BP 7955, Sidi Othman, Casablanca, Morocco

Abstract. In this paper, we study the multi-region SIS discrete-time model which describes the spread of an influenza pandemic in interconnected regions via infection mobility. Our objective from this model, is to suggest in a first case of simulations, the so-called travel-blocking vicinity optimal control strategy aiming to protect susceptible people of a complex of regions tightly close one to each other, while in a second case, we discuss the importance of such strategies when the regions aiming to control are very dispersed. In the theoretical part of the paper, we utilize a discrete version of the pontryagin's maximum principle for the characterization of the travel-blocking optimal control. As for the numerical part, we program the resolution of our multi-points boundary value problem using discrete progressive-regressive iterative schemes, in an example of a domain composed with 100 regions and where the targeted patch includes 4 regions, in the first time grouped and in a second time, dispersed.

Keywords: influenza; optimal contro; multi-regions; discrete-time model; SIS epidemic model; patch.

2010 AMS Subject Classification: 39A05, 39A45, 39A60, 93C35, 93C55.

*Corresponding author

E-mail address: zakaryma@gmail.com

Received March 1, 2020

1. INTRODUCTION

Models in epidemiology have beneficiated of the well-known susceptible-infected-removed (SIR) model devised in [1] for creating other forms of systems that are seen more adapted to describe dynamics of diseases with particular characteristics. We can cite the S-Exposed-IR (SEIR) form as in [2] and that is important when the latent or incubation period is taken into consideration as once been contaminated, individuals are not immediately contagious, also the SIRS form when the immunity is just temporary as in [3]. Other forms of compartment-based models used in different research areas can be found as an example in [4, 5]. In this study, we focus on the SIS form which refers to the case when there is no immunity as in [6]. SIS systems in other research areas such as network security and eco-epidemiology, are also useful to study different phenomena, see as examples, studies in [7, 8]. Other authors preferred the study of SIS model based on discrete-time equations as in [9] and [10]. In fact, as noted in [11], data are often collected in discrete times and this is the main reason behind choosing a discrete-time SIS model here.

Papers [11, 12] proposed new modeling approaches based on multi-regions discrete-time epidemic models to describe the spatial-temporal spread of an epidemic via infection mobility, and they studied the continuous-time versions of their models in particular cases of emerging diseases such as Ebola and Human Immunodeficiency Virus infection and Acquired Immune Deficiency Syndrome (HIV/AIDS) in [13] and [14] respectively. Such systems are also important to show the influence of one region on another. With the introduction of the notion of vicinity and using cellular representations of regions threatened by the epidemic, the authors in [15, 16, 17, 18] investigated the application of those approaches when models are in form of SIR, S-Exposed-IRS (SEIRS), SEIS and SIS discrete equations respectively.

Belik et al. In their paper [19], showed the possibility of the consideration of the factor of mobility when the spatial spread of an epidemic is described using a metapopulation reaction-diffusion model, aiming to show the impact of movement on features of disease dynamics. In fact, as we are concerned about influenza pandemic, there is [20] as example

of study which discussed the role of human mobility in the spread of this disease. In [17], abouelkheir et al. Have proposed a metapopulation-like model for modeling the spread of influenza pandemic based on a SIS model framework. Here, we try to do the same but with the application of the optimal control approach proposed in [22, 23, 24]. More explicitly, the authors in [17] have not treated the case when we have to control a group of areas or a patch but not only one area. Let us try then to clarify the exact difference between a control policy that aims to prevent infection from entering one area or region in a given domain and when this infection has more accessibility to enter many regions or a patch. First, we define a patch as follows.

Let Ω be our global domain of interest, in form of a grid of colored cells, uniform in size and connected via movements of their populations. This is just a simplified representation of such connections and which is useful even in the case when these cells are not necessarily joined together. The cells will represent sub-domains of Ω or regions, or more concretely, cities or countries, and we denote them by $(C_{pq})_{p,q=1,..,m}$. Let then the patch be defined by $P = \bigcup_{p,q=1}^{n} C_{pq}$ with $n < m$, subject to a sirs discrete-time system associated to C_{pq} and with optimal controls functions introduced as effectiveness rates of the travel-blocking operations followed between p and its neighbors. We will need thereafter, the definition of a vicinity set V_{pq} which is composed by all neighboring cells of C_{pq} and which are denoted by $(C_{rs})_{r=p+k,s=q+k'}$ with $(k,k') \in \{-1,0,1\}^2$ except when $k = k' = 0$. Thus, instead of showing the impact of the travel-blocking vicinity optimal approach on reducing contacts between susceptible people of a targeted cell C_{pq} and infected people coming from cells of its vicinity as done in [22], we will be interested here to prove the effectiveness of such policies when they are applied in the borders of the targeted regions chain P with C_{rs} of V_{pq}.

A discrete version of the pontryagin's maximum principle is utilized for the characterization of the travel-blocking optimal control. We illustrate the numerical simulations of an example in a domain composed with 100 regions while the patch aiming to control includes includes 4 regions, in a first time grouped and in a second time, dispersed.

2. A Discrete-Time Multi-Regions Epidemic Model

The domain of study Ω is defined as $\bigcup_{p,q=1}^{m} C_{pq}$. The numbers of susceptibles and infectives associated to a cell C_{pq} are represented by the states $S_i^{C_{pq}}$ and $I_i^{C_{pq}}$, and we note that the transition between them, is probabilistic, with probabilities being determined by the observed characteristics of specific diseases. In addition to death, there are population movements among these three epidemiological compartments, from time unit i to time $i+1$. Susceptible individuals are assumed to be not yet infected but can be infected only through contacts with infected people from V_{pq}, thus, the infection transmission is assumed to occur between individuals present in a given cell C_{pq}, and is given by

$$\sum_{C_{rs}\in V_{pq}} \beta_{rs} I_i^{C_{rs}} S_i^{C_{pq}}$$

Where β_{rs} is the constant proportion of adequate contacts between a susceptible from a Cell C_{pq} and an Infective coming from its neighbor Cell $C_{rs} \in V_{pq}$ with

$V_{pq}=\left\{C_{rs} \in \Omega / r = p+k, s = q+k', (k,k') \in \{-1,0,1\}^2\right\} \setminus C_{pq}$.

SIS dynamics associated to domain or cell C_{pq} are described based on the following multi-cells discrete time model

For $p,q = 1,\ldots,M$, we have

$$\begin{aligned} S_{i+1}^{C_{pq}} &= S_i^{C_{pq}} - \beta_{pq} I_i^{C_{pq}} S_i^{C_{pq}} - \sum_{C_{rs}\in V_{pq}} \beta_{rs} I_i^{C_{rs}} S_i^{C_{pq}} \\ &\quad -dS_i^{C_{pq}} + \theta I_i^{C_{pq}} \end{aligned} \tag{1}$$

$$\begin{aligned} I_{i+1}^{C_{pq}} &= I_i^{C_{pq}} + \beta_{pq} I_i^{C_{pq}} S_i^{C_{pq}} + \sum_{C_{rs}\in V_{pq}} \beta_{rs} I_i^{C_{rs}} S_i^{C_{pq}} \\ &\quad -(\alpha+\theta+d) I_i^{C_{pq}} \end{aligned} \tag{2}$$

$i = 0,\ldots,N-1$

with $S_0^{C_{pq}} > 0$ and $I_0^{C_{pq}} \geq 0$ are the given initial conditions.

Here, $d > 0$ is the natural death rate while $\alpha > 0$ is the death rate due to the infection, $\theta > 0$ denotes the recovery rate. By assuming that is all regions are occupied by homogeneous populations, α, d and θ are considered to be the same for all cells of Ω.

3. A TRAVEL-BLOCKING VICINITY OPTIMAL CONTROL APPROACH

Let $I=\{1,2,...,m\}$, $I_h \subset i$ a subset of I, and consider $P=\left\{C_{pq}/p,q \in i_h\right\}$ denoting a patch of controlled cells, with its complementary in Ω, defined as
$\bar{P}=\left\{C_{ij}/i,j \in I\backslash I_h\right\}$.

The main goal of the travel-blocking vicinity optimal control approach is to restrict movements of infected people coming from the set V_{pq} and aiming to reach the patch P without including cells C_{rs} which belong to $V_{pq}\bigcap P$. For this, we introduce control variables $u^{pqC_{rs}}$ which limits contacts between susceptible of the patch P and infected individuals from cells C_{rs} which belong to $V_{pq}\bigcap \bar{P}$.

In this section, we introduce controls variables in the above mentioned model to restrict contacts between susceptible people of the controlled cells $C_{pq} \in P$ and infected ones which belong to $C_{rs} \in \bar{P} \cap V_{pq}$. Then, for a given cell $C_{pq} \in P$, the discrete-time system (1)-(2) becomes

$$\begin{aligned} S_{i+1}^{C_{pq}} &= S_i^{C_{pq}} - \beta_{pq} I_i^{C_{pq}} S_i^{C_{pq}} - \sum_{C_{rs}\in P\cap V_{pq}} \beta_{rs} I_i^{C_{rs}} S_i^{C_{pq}} \\ &\quad - \sum_{C_{rs}\in \bar{P}\cap V_{pq}} u_i^{pqC_{rs}} \beta_{rs} I_i^{C_{rs}} S_i^{C_{pq}} - dS_i^{C_{pq}} + \theta I_i^{C_{pq}} \end{aligned} \tag{3}$$

$$\begin{aligned} I_{i+1}^{C_{pq}} &= I_i^{C_{pq}} + \beta_{pq} I_i^{C_{pq}} S_i^{C_{pq}} + \sum_{C_{rs}\in P\cap V_{pq}} \beta_{rs} I_i^{C_{rs}} S_i^{C_{pq}} \\ &\quad + \sum_{C_{rs}\in \bar{P}\cap V_{pq}} u_i^{pqC_{rs}} \beta_{rs} I_i^{C_{rs}} S_i^{C_{pq}} - (d+\alpha+\theta) I_i^{C_{pq}} \end{aligned} \tag{4}$$

$i=0,...,N-1$

Since our goal concerns the minimization of the number of the infected people and the cost of the vicinity optimal control approach, we consider an optimization criterion associated to the patch P, and we define it by the following objective function

$$J_P(u) = \sum_{C_{pq}\in P} \left[A_1 I_N^{C_{pq}} + \sum_{i=0}^{N-1} \left(A_1 I_i^{C_{pq}} + \sum_{C_{rs}\in \bar{P}\cap V_{pq}} \frac{A_{rs}}{2} (u_i^{pqC_{rs}})^2 \right) \right] \tag{5}$$

Where $A_1 > 0$ and $A_{rs} > 0$ are the constant severity weights associated to the number of infected individuals and controls respectively.

we note that here,

$$u = \left(u_i^{pqC_{rs}}\right)_{C_{rs}\in\bar{P}\bigcap V_{pq}, i=1,...,n-1, p,q\in I_h}$$

which belongs to the control set U_P defined as

$$U_P = \left\{u/u^{min} \leq u_i^{pqC_{rs}} \leq u^{max},\, i = 1,...,N-1,\, C_{rs} \in \bar{P}\cap V_{pq}\right\}$$

Then, we seek optimal control u such that

$$J_P(u^*) = min\{J_P(u)/u \in U_P\}$$

The sufficient conditions for the existence of optimal controls in the case of discrete-time epidemic models have been announced in [25] and [26].

As regards to the necessary conditions and the characterization of our discrete optimal control, we use a discrete version of the pontryagin's maximum principle [27].

For this, we define an hamiltonian $\mathscr{H}$ associated to a patch P by

$$\begin{aligned}
\mathscr{H} &= \sum_{C_{pq}\in P}\Bigg[A_1 I_i^{C_{pq}} + \sum_{C_{rs}\in\bar{P}\cap V_{pq}} \frac{A_{rs}}{2}(u_i^{pqC_{rs}})^2 \\
&+ \zeta_{1,i+1}^{C_{pq}}\Bigg(S_i^{C_{pq}} - \beta_{pq} I_i^{C_{pq}} S_i^{C_{pq}} - \sum_{C_{rs}\in P\cap V_{pq}} \beta_{rs} I_i^{C_{rs}} S_i^{C_{pq}} \\
&\quad - \sum_{C_{rs}\in\bar{P}\cap V_{pq}} u_i^{pqC_{rs}} \beta_{rs} I_i^{C_{rs}} S_i^{C_{pq}} - d S_i^{C_{pq}} + \theta I_i^{C_{pq}}\Bigg) \\
&+ \zeta_{2,i+1}^{C_{pq}}\Bigg(I_i^{C_{pq}} + \beta_{pq} I_i^{C_{pq}} S_i^{C_{pq}} + \sum_{C_{rs}\in P\cap V_{pq}} \beta_{rs} I_i^{C_{rs}} S_i^{C_{pq}} \\
&\quad + \sum_{C_{rs}\in\bar{P}\cap V_{pq}} u_i^{pqC_{rs}} \beta_{rs} I_i^{C_{rs}} S_i^{C_{pq}} - (d+\alpha+\theta) I_i^{C_{pq}}\Bigg)\Bigg]
\end{aligned} \tag{7}$$

$i = 0, ..., N-1$

with $\zeta_{k,i}^{C_{pq}}$, $k = 1,2$, the Adjoint Variables Associated to $S_i^{C_{pq}}$ and $I_i^{C_{pq}}$ Respectively, and Defined Based on Formulations of the Following Theorem.

Theorem: (Necessary Conditions & Characterization). Given Otimal Controls $u^{pqC_{rs}*}$ and Solutions $S^{C^*_{pq}}$ and $I^{C^*_{pq}}$, there Exists $\zeta_{k,i}^{C_{pq}}$, $i = 0...N$, $k = 1,2$, the Adjoint Variables Satisfying the Following Equations

$$\begin{aligned}
\triangle\zeta_{1,i}^{C_{pq}} &= -\left[(1-d)\,\zeta_{1,i+1}^{C_{pq}} + \left(\beta_{pq} I_i^{C_{pq}} + \sum_{C_{rs}\in P\cap V_{pq}} \beta_{rs} I_i^{C_{rs}} + \sum_{C_{rs}\in \bar{P}\cap V_{pq}} u_i^{pqC_{rs}} \beta_{rs} I_i^{C_{rs}}\right) \times \left(\zeta_{2,i+1}^{C_{pq}} - \zeta_{1,i+1}^{C_{pq}}\right)\right] \\
\triangle\zeta_{2,i}^{C_{pq}} &= -\left[A_1 + \beta_{pq} S_i^{C_{pq}} \left(\zeta_{2,i+1}^{C_{pq}} - \zeta_{1,i+1}^{C_{pq}}\right) + (1-d-\alpha)\,\zeta_{2,i+1}^{C_{pq}} + \theta\left(\zeta_{1,i+1}^{C_{pq}} - \zeta_{2,i+1}^{C_{pq}}\right)\right]
\end{aligned} \tag{8}$$

with $\zeta_{1,N}^{C_{pq}} = 0, \zeta_{2,N}^{C_{pq}} = A_1$ are the transversality conditions.

In addition

$$u_i^{pqC_{rs}*} = min\left(max\left(u^{min}, \frac{(\zeta_{1,i+1}^{C_{pq}} - \zeta_{2,i+1}^{C_{pq}})\beta_{rs} I_i^{C_{rs}*} S_i^{C_{pq}*}}{A_{rs}}\right), u^{max}\right),$$

$i = 0, ..., N-1, C_{rs} \in V_{pq}$

Proof. Using a discrete version of the Pontryagin's Maximum Principle in [11],[12],[27], and setting $S^{C_{pq}} = S^{C_{pq}*}$, $I^{C_{pq}} = I^{C_{pq}*}$ and $u^{pqC_{rs}} = u^{pqC_{rs}*}$ we obtain the following adjoint equations

$$\begin{aligned}
\triangle\zeta_{1,i}^{C_{pq}} &- \frac{\partial\mathscr{H}}{\partial S_i^{C_{pq}}} \\
&= -[(1-d)\,\zeta_{1,i+1}^{C_{pq}} + \left(\beta_{pq} I_i^{C_{pq}} + \sum_{C_{rs}\in P\cap V_{pq}} \beta_{rs} I_i^{C_{rs}}\right. \\
&+ \left.\sum_{C_{rs}\in \bar{P}\cap V_{pq}} u_i^{pqC_{rs}} \beta_{rs} I_i^{C_{rs}} \quad \times \quad \left(\zeta_{2,i+1}^{C_{pq}} - \zeta_{1,i+1}^{C_{pq}}\right)\right]
\end{aligned}$$

$$\begin{aligned}
\triangle\zeta_{2,i}^{C_{pq}} &= -\frac{\partial\mathscr{H}}{\partial I_i^{C_{pq}}} \\
&= -\left[A_1 + \beta_{pq} S_i^{C_{pq}} \left(\zeta_{2,i+1}^{C_{pq}} - \zeta_{1,i+1}^{C_{pq}}\right)\right. \\
&+ \left.(1-d-\alpha)\,\zeta_{2,i+1}^{C_{pq}} + \theta\left(\zeta_{1,i+1}^{C_{pq}} - \zeta_{2,i+1}^{C_{pq}}\right)\right.
\end{aligned}$$

$S_0^{C_{pq}}$	$I_0^{C_{pq}}$	α	β	d	θ
50	0	0.002	0.0001	0.0001	0.003

TABLE 1. Parameters values of α, β, θ and d with the initial conditions $S_0^{C_{pq}}$ and $I_0^{C_{pq}}$ associated to any cell C_{pq} of Ω.

with $\triangle\zeta_{k,i} = \zeta_{k,i+1} - \zeta_{k,i},\ k = 1,2;$ the Difference Operator, and $\zeta_{1,N}^{C_{pq}} = 0, \zeta_{2,N}^{C_{pq}} = A_1;$ the Transversality Conditions.

In Order to Obtain the Optimality Condition, we Calculate the Derivative of H with Respect to $u_i^{pqC_{rs}}$, and we Set it Equal to Zero

$$\frac{\partial \mathscr{H}}{\partial u_i^{pqC_{rs}}} = A_{rs}u_i^{pqC_{rs}} - \zeta_{1,i+1}^{C_{pq}}\beta_{rs}I_i^{C_{rs}}S_i^{C_{pq}} + \zeta_{2,i+1}^{C_{pq}}\beta_{rs}I_i^{C_{rs}}S_i^{C_{pq}} = 0$$

Then, we Obtain

$$u_i^{pqC_{rs}} = \frac{(\zeta_{1,i+1}^{C_{pq}} - \zeta_{2,i+1}^{Cpq})\beta_{rs}I_i^{C_{rs}}S_i^{C_{pq}}}{A_{rs}}$$

By the Bounds in U_P, We Finally Obtain the Characterization of The Optimal Controls $u_i^{pqC_{rs}^*}$ as

$$u_i^{pqC_{rs}*} = min\left(max\left(u^{min}, \frac{(\zeta_{1,i+1}^{C_{pq}} - \zeta_{2,i+1}^{C_{pq}})\beta_{rs}I_i^{C_{rs}*}S_i^{C_{pq}*}}{A_{rs}}\right), u^{max}\right),$$
$$i = 0,...,N-1, C_{rs} \in V_{pq}$$

□

4. RESULTS

For the numerical method followed in this part, we refer to [15, 16, 17, 18, 21, 22], to understand our programming code used in the simulations below. However, here are some important information to make our comments clearer.

- $M = 10$; $\Omega = 10 \times 10$ grid.

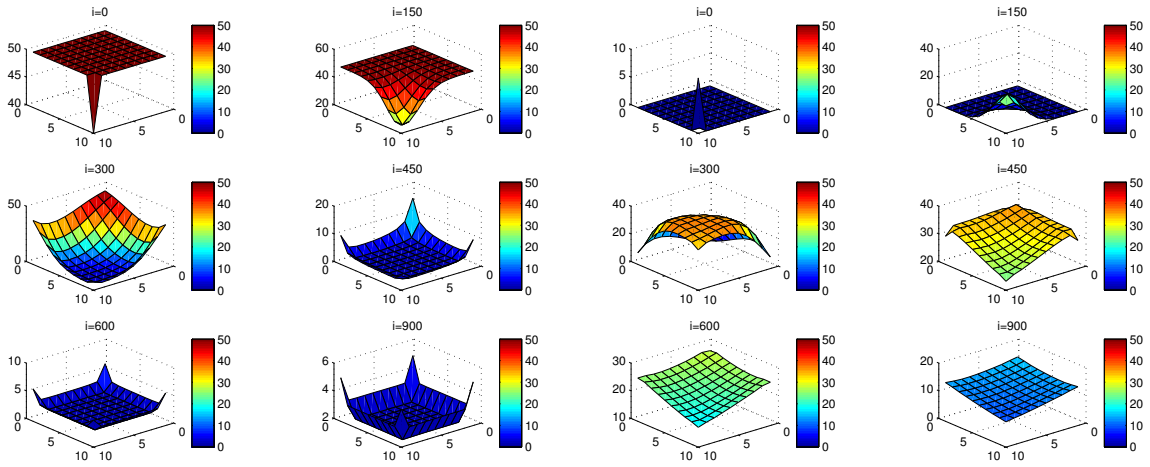

Figure 1. Behaviors of the numbers of susceptible and infected people of Ω in the absence of controls. The left-hand side concerns $S^{C_{pq}}$ while the right-hand side concerns $I^{C_{pq}}$.

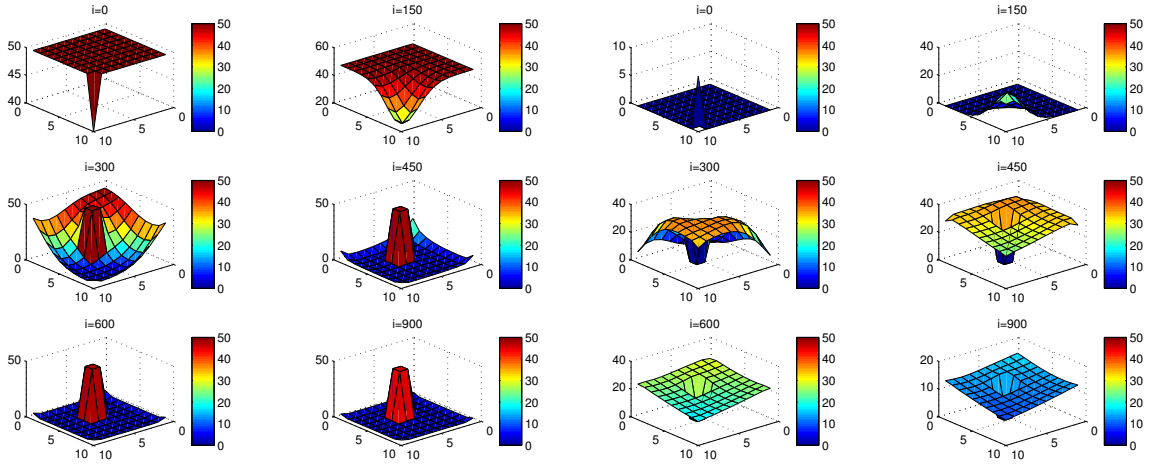

Figure 2. Case of a patch as a complex of 4 cells: Behaviors of the numbers of susceptible and infected people of Ω in the presence of controls. The left-hand side concerns $S^{C_{pq}}$ while the right-hand side concerns $I^{C_{pq}}$.

- C_{1010}, the source infection Cell, is located at the lower-right corner of Ω.
- $S_0^{C_{pq}} = 50$ except $S_0^{C_{1010}} = 40$.
- $I_0^{C_{pq}} = 0$ except $I_0^{C_{1010}} = 10$.
- In a first case, we define a patch as a complex of 4 regions tightly close one to each other, and then, we consider the set containing the cells $C_{64}, C_{65}, C_{55}, C_{54}$.

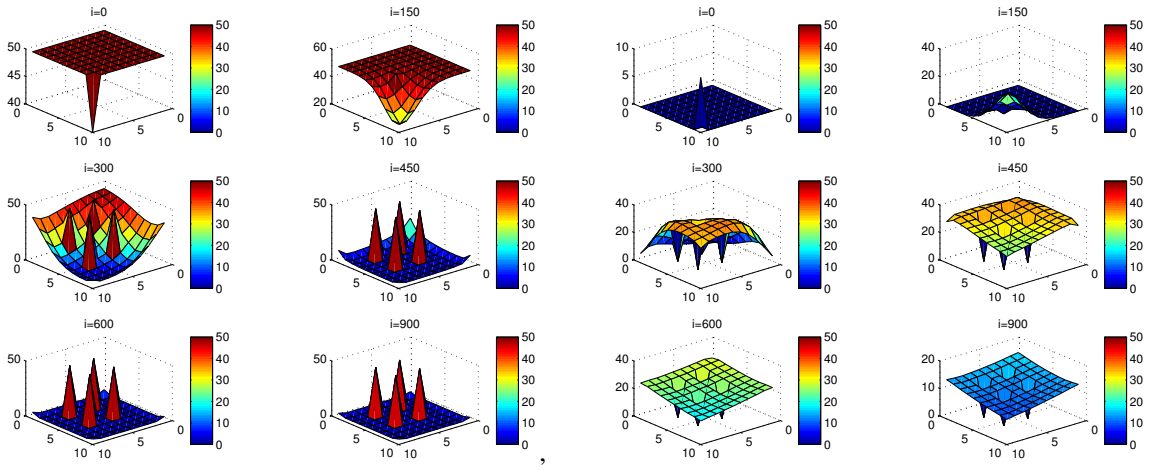

Figure 3. Case of a patch as a group of 4 dispersed cells: Behaviors of the numbers of susceptible and infected people of Ω in the presence of controls. The left-hand side concerns $S^{C_{pq}}$ while the right-hand side concerns $I^{C_{pq}}$.

- In a second case, we define a patch as a group of 4 dispersed regions, and then, we consider the set containing the cells $C_{43}, C_{73}, C_{76}, C_{46}$.

For other details, see table 1.

Figure 1. In both sides illustrates simulations of $S^{C_{pq}}$ and $I^{C_{pq}}$ respectively When there is yet no control strategy followed for the prevention of the epidemic. As the infection is supposed to start from the cell C_{1010}, we can observe at the left-hand side of figure 1. that at instant $i = 150$, the number $S^{C_{1010}}$ becomes less important and takes values between 20 and 30, while $S^{C_{pq}}$ in cells of v_{1010}, it takes values close/or equal to 25, and as we move away from v_{1010}, $S^{C_{pq}}$ remains important. At instant $i = 300$, we can observe that in most of cells that are in/or close to v_{1010}, $S^{C_{pq}}$ becomes less important, taking values between 0 and 10, and as we move away from the source of infection, the number of susceptibles in other cells takes values between 20 and 40 except $S^{C_{110}}$ which conserves its value in 50. At instant $i = 450$, $S^{C_{pq}}$ becomes zero except at the opposite corner that contains only 20 susceptible individuals while in opposite borders, $S^{C_{pq}}$ takes only the value 5 as cells in these borders have vicinity sets smaller than other cells and then the infection takes a long time to reach them. Finally, at last instants, $S^{C_{pq}}$ converge to zro

Figure 4. Behavior of the infected population in the controlled patch $P = \{C_{64}, C_{65}, C_{54}, C_{55}\}$ and its neighbor. **(a)** Shapes of $I^{C_{43}}$, $I^{C_{53}}$, $I^{C_{44}}$ and $I^{C_{54}}$. **(b)** Shapes of $I^{C_{63}}$, $I^{C_{73}}$, $I^{C_{74}}$ and $I^{C_{64}}$. **(c)** Shapes of $I^{C_{45}}$, $I^{C_{46}}$, $I^{C_{56}}$ and $I^{C_{55}}$. **(d)** Shapes of $I^{C_{75}}$, $I^{C_{76}}$, $I^{C_{66}}$ and $I^{C_{65}}$.

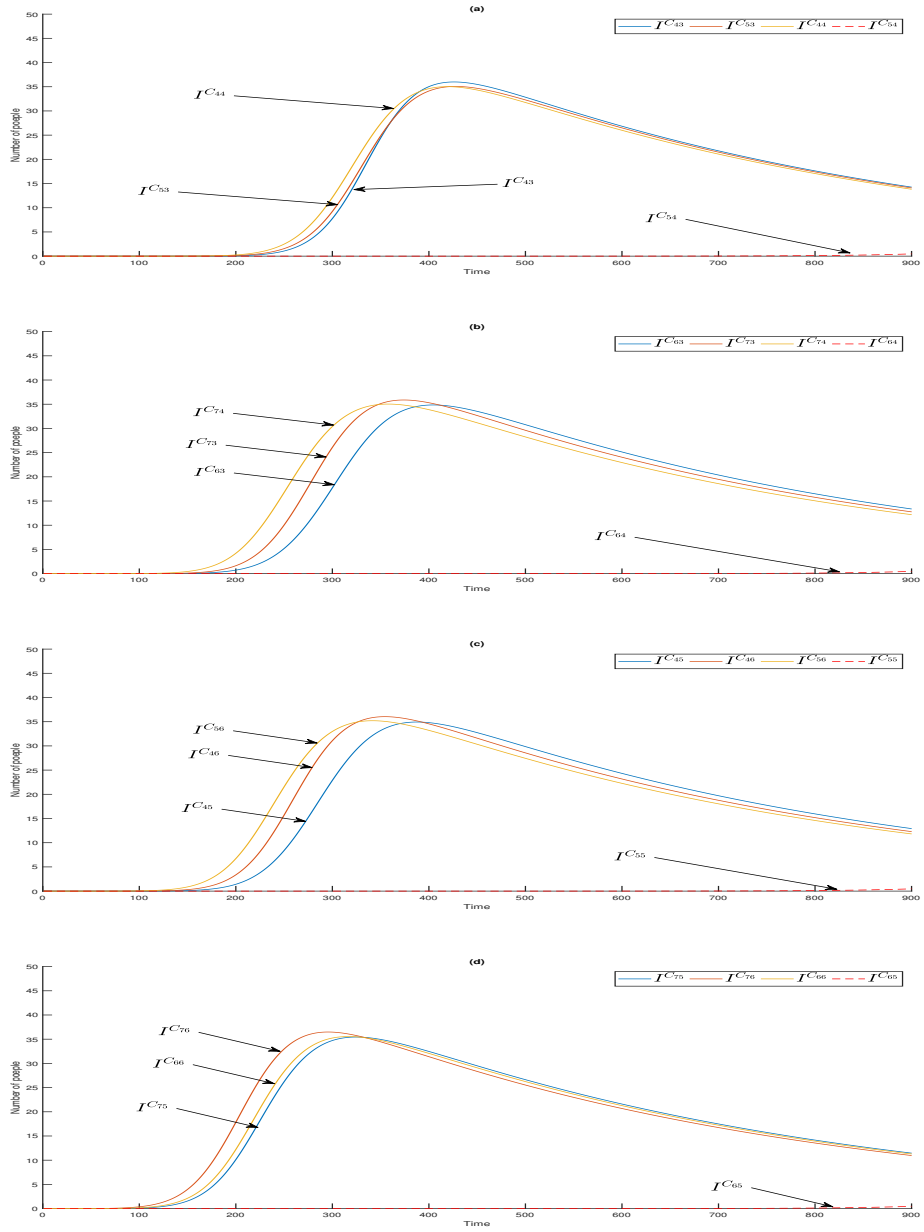

in all cells.

At the left-hand side of figure 1. depicts the rapid spread of the infection in Ω, and we can see that at instant $i = 150$, the number $I^{C_{1010}}$ increases to a bigger value which is close/or equals 25, while $I^{C_{pq}}$ in cells of v_{1010}, it takes values close/or equal to 20, and as we move away from

Figure 5. Behavior of the infected population in the controlled patch $P = \{C_{43}, C_{73}, C_{46}, C_{76}\}$ and its neighbor. **(a)** Shapes of $I^{C_{33}}$, $I^{C_{53}}$, $I^{C_{32}}$, $I^{C_{42}}$, $I^{C_{52}}$, $I^{C_{34}}$, $I^{C_{44}}$, $I^{C_{54}}$ and $I^{C_{43}}$. **(b)** Shapes of $I^{C_{63}}$, $I^{C_{83}}$, $I^{C_{62}}$, $I^{C_{72}}$, $I^{C_{82}}$, $I^{C_{64}}$, $I^{C_{74}}$, $I^{C_{84}}$ and $I^{C_{73}}$. **(c)** Shapes of $I^{C_{36}}$, $I^{C_{56}}$, $I^{C_{35}}$, $I^{C_{45}}$, $I^{C_{55}}$, $I^{C_{37}}$, $I^{C_{47}}$, $I^{C_{57}}$ and $I^{C_{46}}$. **(d)** Shapes of $I^{C_{66}}$, $I^{C_{86}}$, $I^{C_{65}}$, $I^{C_{75}}$, $I^{C_{85}}$, $I^{C_{67}}$, $I^{C_{77}}$, $I^{C_{87}}$ and $I^{C_{76}}$.

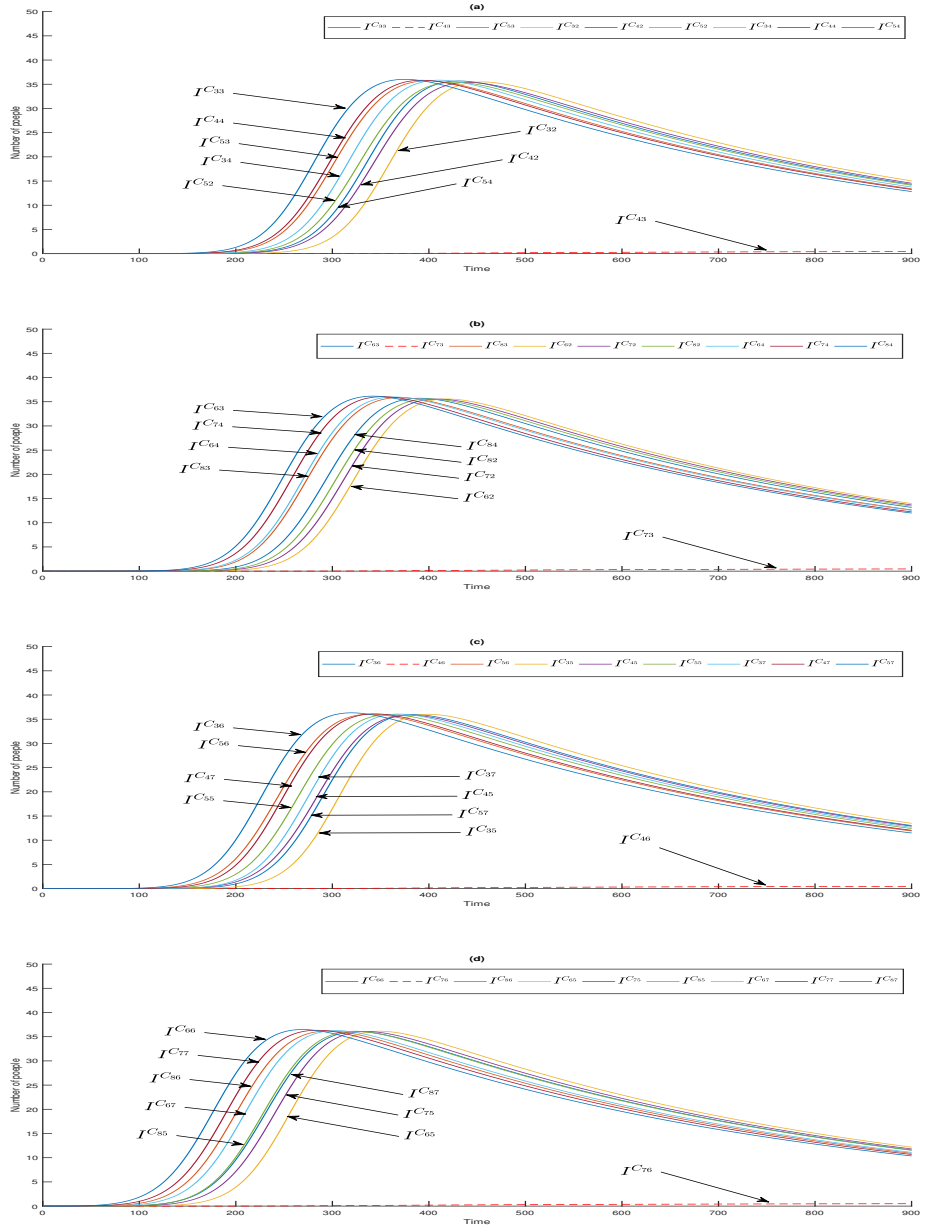

v_{1010}, $I^{C_{pq}}$ remains less important. At instant $i = 300$, we can see that in most cells, $I^{C_{pq}}$ becomes more important, taking values that are close to 35 especially in cells with 8 neighbors, while in few other cells, it takes values that are close to 15. From these numerical results, we can deduce that once the infection arrives to the center or to the cells with 8 cells in their vicinity

sets, the infection becomes more important compared to the case of the previous instant. At instant $i = 450$, $I^{C_{pq}}$ takes values which equal/or are close to 28 or more in cells that are close to the source of infection, and it takes the value 25 in v_{1010} and near to it, and as we move away towards the center and further regions, infection is important with the presence of 32 infected individuals in the 3 opposite corners and which changes to 25 at instant $i = 600$. In fact, at the center of Ω, the number of infected people which has increased to 30 at the previous instant $(i = 450)$, has been reduced as once a cell becomes highly infected, it loses an important number of individuals which die, recover naturally after or become susceptible again, and this can be more deduced from values at further instants.

At both sides of figure 2., we present simulations of the s-i populations when the travel-blocking vicinity optimal control strategy is followed and when the patch aiming to control is defined as the complex of the 4 cells defined in the introduction of this section.. We can observe now at the left-hand side of figure 1. That at instant $i = 150$, the numbers $S^{C_{1010}}$ and $S^{C_{pq}}$ are at most the same as in the case when there was no control strategy. However, the controlled patch P still contains about 50 susceptible people at instant $i = 300$, which is not exactly the same as in the case above in figure 1. Where the number $S^{C_{pq}}$ in p has decreased more significantly. Thus, we can deduce that the travel-blocking vicinity optimal control strategy has proved its effectiveness earlier in time. At instants $i = 450, 600$ and $i = 900$, $S^{C_{pq}}$ in p has decreased by only 2, 4 and 6 people respectively.

as for simulations at the right-hand side of figure 2., we deduce that at instants $i = 0,\ 150$, the numbers $I^{C_{1010}}$ and other $I^{C_{pq}}$ are at most the same as in figure 1. At instant $i = 300$, we can see that in most cells, $I^{C_{pq}}$ is also similar to the case in figure 1. But the controlled patch P is still not really infected and contains only about one infected individual, and the number remains always not important at further instants.

At both sides of figure 3., we treat again simulations of the s-i populations when the travel-blocking vicinity optimal control strategy is followed, but when the patch is defined by the 4

dispersed cells defined in the introduction of this section. Similar conclusions as in the previous figure are again manifested here. In fact, at final time in the left-hand side of this figure, the four cells in the controlled patch P, have contained equally numbers that are close to 50 susceptible people, while in the right-hand side of the same figure, they have not contained any important numbers of infected people, all meaning there was no real observable change.

Figures 4. And 5. Present more clearly the behaviors of numbers of infected people in cells that belong to vicinities of the controlled patches defined by the sets $\{C_{64}, C_{65}, C_{54}, C_{55}\}$ and $\{C_{43}, C_{73}, C_{46}, C_{76}\}$ respectively, while the dashed curves in all subfigures (a), (b), (c) and (d) in figure 4. And 5., present numbers of infected people in these controlled groups of regions.

To give a clearer idea of figures 4, we will describe each sub-figure separately. In (a), the first rising curve is that associated with $I^{C_{44}}$, followed by the curve associated with $I^{C_{53}}$, then the curve of $I^{C_{43}}$. Finally, the curve associated with $I^{C_{54}}$ which is almost zero. In (b), the first ascending curve is that associated with $I^{C_{74}}$, followed by the curve associated with $I^{C_{73}}$, then the curve of $I^{C_{63}}$. Finally, the curve associated with $I^{C_{64}}$ which is almost zero. In (c), the first ascending curve is that associated with $I^{C_{56}}$, followed by the curve associated with $I^{C_{46}}$, then the curve of $I^{C_{45}}$. Finally, the curve associated with $I^{C_{55}}$ which is almost zero. In (d), the first ascending curve is that associated with $I^{C_{76}}$, followed by the curve associated with $I^{C_{66}}$, then the curve of $I^{C_{75}}$. Finally, the curve associated with $I^{C_{65}}$ which is almost zero.

As regards figure 5, we have in subfigure (a), the first rising curve is that associated with $I^{C_{33}}$, followed by the curve associated with $I^{C_{44}}$, then the curve of $I^{C_{53}}$, followed by the curve associated with $I^{C_{34}}$, then the curve of $I^{C_{52}}$, and then the curve of $I^{C_{54}}$, followed by the curve associated with $I^{C_{42}}$, then the curve of $I^{C_{32}}$. Finally, the curve associated with $I^{C_{43}}$ which is almost zero. In (b), the first ascending curve is the one associated with $I^{c_{63}}$, followed by the curve associated with $I^{c_{74}}$, then the curve of $I^{c_{64}}$, follow the curve associated with $I^{c_{83}}$, then from the curve of $I^{c_{84}}$, then from the curve of $I^{c_{82}}$, followed by the curve associated with $I^{c_{72}}$, then the curve of $I^{c_{62}}$. Finally, the curve associated with $I^{c_{73}}$ is almost zero. In (c), the first ascending curve is the one associated with $I^{c_{36}}$, followed by the curve associated with $I^{c_{56}}$, then the curve of $I^{c_{47}}$, followed by the curve associated with $I^{c_{55}}$, then of the curve of $I^{c_{37}}$, then of the curve of $I^{c_{45}}$, followed

by the curve associated with $I^{c_{57}}$, then the curve of $I^{c_{35}}$. Finally, the curve associated with $I^{c_{46}}$ which is almost zero. In (d), the first ascending curve is the one associated with $I^{c_{66}}$, followed by the curve associated with $I^{c_{77}}$, then the curve of $I^{c_{86}}$, followed by the curve associated with $I^{c_{67}}$, then of the curve of $I^{c_{85}}$, then of the curve of $I^{c_{87}}$, followed by the curve associated with $I^{c_{75}}$, then the curve of $I^{c_{65}}$. Finally, the curve associated with $I^{c_{76}}$ which is almost zero.

We note that cells belonging to the vicinity of the first patch that is formed of tightly interconnected regions, are $C_{43}, C_{44}, C_{45}, C_{46}, C_{53}, C_{56}, C_{63}, C_{66}, C_{73}, C_{74}, C_{75}$ and C_{76}, while cells belonging to the vicinity of the second patch that is formed of dispersed regions are $C_{32}, C_{33}, C_{34}, C_{35}, C_{36}$, $C_{37}, C_{42}, C_{44}, C_{45}, C_{47}, C_{52}, C_{53}, C_{54}, C_{55}, C_{56}, C_{57}, C_{62}, C_{63}, C_{64}, C_{65}, C_{66}, C_{67}, C_{72}, C_{74}, C_{75}, C_{77}, C_{82}$, $C_{83}, C_{84}, C_{85}, C_{86}$ and C_{87}. We can remark that cells of the second patch, especially C_{73} and C_{76}, have neighboring cells located in the 8th line of Ω and this location is closer to the source of infection C_{1010}, this leads to the important values that infection can reach in some cells such as C_{87}, C_{77} and C_{86} as observed in the subfigure (d) of figure 5., while the maximal peaks of other cells in the same simulation, take lesser values. This conclusion can also be drawn from subfigure (d) of figure 4. And where neighboring cells C_{76}, C_{66} and C_{75} of cell C_{65} that belong to the first patch, all have more important peaks than other cells. Similar results are observed from all other subfigures of the two figures, all meaning that the more a region is close to the source of infection, the more the infection can reach serious peaks. On the other hand, we can also remark that curves in figure 5. Are close to each other more than the ones in the first figure, and this can be simply explained by the fact that in figure 5., the dispersion of cells of the second patch allow them higher number of neighbors, and then, once the infection arrives to these neighboring cells, their numbers of infected people show similar behaviors and the values are closer to each other, but in figure 4. A neighboring cell has in turn one or two neighboring cells in the patch, and this leads to larger difference in peak values.

We can understand from these simulations that the introduced optimal controls have been effective in preventing the epidemic to enter those patches as the infection does not increase and stabilize in the level of the zero value along the optimal control strategy period while it remains important only in the neighboring cells.

These deductions are valid either for the case of a patch with many cells in its vicinity as in the first example of set $\{C_{43}, C_{73}, C_{46}, C_{76}\}$ in figure 4., or for the case of the patch that has lesser neighboring cells as in the second set $\{C_{64}, C_{65}, C_{54}, C_{55}\}$ in figure 5., and this proves the effectiveness of travel restrictions regardless of the number of cells in vicinity sets.

5. Conclusion

In order to exhibit the impact of influenza pandemic infection coming from the vicinity of a patch or a group of regions, we studied dynamics of a SIS discrete-time multi-regions epidemic model after the introduction of a control that is associated to the travel-blocking vicinity optimal control approach. Finally, we demonstrated that such control policies are always effective regardless the form of the patch.

Conflict of Interests

The author(s) declare that there is no conflict of interests.

References

[1] W. O. Kermack, A. G. McKendrick, A contribution to the mathematical theory of epidemics, Proc. R. Soc. Lond. A. 115 (1927), 700–721.

[2] A. Korobeinikov, Lyapunov functions and global properties for SEIR and SEIS epidemic models, Math. Med. Biol. 21 (2004), 75–83.

[3] S. Gonçalves, G. Abramson, M.F.C. Gomes, Oscillations in SIRS model with distributed delays, Eur. Phys. J. B. 81 (2011), 363–371.

[4] S. Bidah, O. Zakary, M. Rachik, Stability and Global Sensitivity Analysis for an Agree-Disagree Model: Partial Rank Correlation Coefficient and Latin Hypercube Sampling Methods, Int. J. Differ. Equations. 2020 (2020), 5051248.

[5] H. Boutayeb, S. Bidah, O. Zakary, M. Rachik, A New Simple Epidemic Discrete-Time Model Describing the Dissemination of Information with Optimal Control Strategy, Discrete Dyn. Nat. Soc. 2020 (2020), 7465761.

[6] A. Gray, D. Greenhalgh, X. Mao, J. Pan, The SIS epidemic model with Markovian switching, J. Math. Anal. Appl. 394 (2012), 496–516.

[7] J. Kim, S. Radhakrishnan, J. Jang, Cost Optimization in SIS Model of Worm Infection, ETRI J. 28 (2006), 692–695.

[8] S. Sun, C. Yuan, Analysis of eco-epidemiological SIS model with epidemic in the predator, Chinese J. Engineering Math. 22 (2005), 30-34.

[9] C. Castillo-Chavez, A. A. Yakubu, Discrete-time SIS models with complex dynamics. Nonlinear Anal., Theory Methods Appl. 47(7)(2001), 4753-4762.

[10] A. A. Yakubu, Allee effects in a discrete-time SIS epidemic model with infected newborns. J. Difference Equ. Appl. 13 (4) (2007), 341-356.

[11] O. Zakary, M. Rachik, I. Elmouki, On the analysis of a multi-regions discrete SIR epidemic model: an optimal control approach, Int. J. Dynam. Control. 5 (2017), 917–930.

[12] O. Zakary, M. Rachik, I. Elmouki, A new analysis of infection dynamics: multi-regions discrete epidemic model with an extended optimal control approach, Int. J. Dynam. Control. 5 (2017), 1010–1019.

[13] O. Zakary, M. Rachik, I. Elmouki, A multi-regional epidemic model for controlling the spread of Ebola: awareness, treatment, and travel-blocking optimal control approaches, Math. Meth. Appl. Sci. 40 (2017), 1265–1279.

[14] O. Zakary, A. Larrache, M. Rachik, I. Elmouki, Effect of awareness programs and travel-blocking operations in the control of HIV/AIDS outbreaks: a multi-domains SIR model, Adv Differ Equ. 2016 (2016), 169.

[15] O. Zakary, M. Rachik, I. Elmouki, A new epidemic modeling approach: Multi-regions discrete-time model with travel-blocking vicinity optimal control strategy. Infect. Dis. Model. 2 (3) (2017), 304-322.

[16] F. El Kihal, M. Rachik, O. Zakary, I. Elmouki, A multi-regions SEIRS discrete epidemic model with a travel-blocking vicinity optimal control approach on cells. Int. J. Adv. Appl. Math. Mech. 4 (3) (2017), 60-71.

[17] I. Abouelkheir, M. Rachik, O. Zakary, I. Elmouki, A multi-regions SIS discrete influenza pandemic model with a travel-blocking vicinity optimal control approach on cells. Amer. J. Comput. Appl. Math. 7 (2) (2017), 37-45.

[18] K. Chouayakh, M. Rachik, O. Zakary, I. Elmouki, A multi-regions SEIS discrete epidemic model with a travel-blocking vicinity optimal control approach on cells. J. Math. Comput. Sci. 7 (3)(2017), 468-484.

[19] V. Belik, T. Geisel, D. Brockmann, Natural Human Mobility Patterns and Spatial Spread of Infectious Diseases, Phys. Rev. X. 1 (2011), 011001.

[20] S. Merler, M. Ajelli, The role of population heterogeneity and human mobility in the spread of pandemic influenza. Proc. R. Soc. Lond. B., Biol. Sci. 277 (1681) (2010), 557-565.

[21] I. Abouelkheir, F. El Kihal, M. Rachik, O. Zakary, I. Elmouki, A multi-regions SIRS discrete epidemic model with a travel-blocking vicinity optimal control approach on cells. Br. J. Math. Comput. Sci. 20 (4) (2017), 1-16.

[22] O. Zakary, M. Rachik, I. Elmouki, S. Lazaiz, A multi-regions discrete-time epidemic model with a travel-blocking vicinity optimal control approach on patches. Adv. Difference Equ. 2017 (2017), 120.

[23] S. Bidah, M. Rachik, O. Zakary, H. Boutayeb, I. Elmouki, Travel-blocking Optimal Control Policy on Borders of a Chain of Regions Subject to SIRS Discrete Epidemic Model, Asian J. Res. Infect. Dis. 1 (2) (2018), AJRID.44975.

[24] O. Zakary, S. Bidah, M. Rachik, I. Elmouki, Cell and patch vicinity travel restrictions in a multi-regions SI discrete epidemic control model. Int. J. Adv. Appl. Math. Mech. 6 (2019), 30-41.

[25] D. Wandi, R. Hendon, B. Cathey, E. Lancaster, R. Germick. Discrete time optimal control applied to pest control problems. Involve, 7 (4) (2014), 479-489.

[26] K. Dabbs, Optimal control in discrete pest control models, Ph.D. thesis, University of Tennessee, 2010.

[27] S.P. Sethi, Optimal control theory: applications to management science and economics, Third edition, Springer, Cham, 2019.